JVST A
Journal of Vacuum Science & Technology A

ARTICLE

avs.scitation.org/journal/jva

Effect of O_2 plasma exposure time during atomic layer deposition of amorphous gallium oxide

Cite as: J. Vac. Sci. Technol. A **39**, 052408 (2021); doi: 10.1116/6.0001207
Submitted: 10 June 2021 · Accepted: 27 July 2021 ·
Published Online: 2 September 2021

View Online

Export Citation

CrossMark

Hanno Kröncke,[1] Florian Maudet,[1,a)] Sourish Banerjee,[1] Jürgen Albert,[1] Sven Wiesner,[1] Veeresh Deshpande,[1] and Catherine Dubourdieu[1,2,a)]

AFFILIATIONS

[1]Helmholtz-Zentrum-Berlin für Materialien und Energy GmbH, Institute "Functional Oxides for Energy Efficient Information Technology," Hahn-Meitner-Platz 1, 14109 Berlin, Germany
[2]Physical Chemistry, Freie Universität Berlin, Arnimallee 22, 14195 Berlin, Germany

Note: This paper is part of the 2022 Special Topic Collection on Atomic Layer Deposition (ALD).
[a)]**Electronic addresses:** florian.maudet@helmholtz-berlin.de and catherine.dubourdieu@helmholtz-berlin.de

ABSTRACT

Amorphous gallium oxide thin films were grown by plasma-enhanced atomic layer deposition on (100) silicon substrates from trimethylgallium $Ga(CH_3)_3$ precursor and oxygen plasma. At 200 °C, the growth per cycle is in the range of 0.65–0.70 Å for O_2 plasma exposure times ranging from 3 up to 30 s during each cycle. The effect of O_2 plasma exposure times on the interfacial SiO_x regrowth and the electrical properties was investigated. *In situ* spectroscopic ellipsometry shows that the SiO_x regrowth occurs during the first three cycles and is limited to 0.27 nm for plasma times as long as 30 s. Increasing the O_2 plasma exposure during each ALD cycle leads to a drastic decrease in the leakage current density (more than 5 orders of magnitude for 30 nm films), which is linked to the suppression of oxygen vacancy states as evidenced by spectroscopic ellipsometry. Interestingly, an increase in the dielectric constant with increasing O_2 plasma exposure time is observed, reaching a value of $\varepsilon_r \sim 14.2$, larger than that of single crystalline β-Ga_2O_3. This study highlights the crucial role of oxygen plasma exposure time in the control and tuning of the electrical properties of amorphous gallium oxide films.

© 2021 Author(s). All article content, except where otherwise noted, is licensed under a Creative Commons Attribution (CC BY) license (http://creativecommons.org/licenses/by/4.0/). https://doi.org/10.1116/6.0001207

I. INTRODUCTION

Ga_2O_3 crystallizes in five different polymorphs, among which the monoclinic β-phase is the stable phase at room temperature and atmospheric pressure.[1] It is an attractive ultrawide bandgap (~4.9 eV) semiconductor, which can be intentionally donor-doped with a large range of accessible electron carrier densities (from $\sim1\times10^{15}$ to $>1\times10^{20}$ cm^{-3}) and with a large electrical breakdown field of ~8 MV/cm.[2] In addition, it can be grown as large single crystals at a relatively low cost from the liquid phase.[3–5] The growth and properties of β-Ga_2O_3 have been investigated in single crystals, thin films, and nanostructures with a renewed interest in the past few years as indicated by the strong increase in related publications.[2] As a crystalline material, there are several highly promising applications such as high-power electronics, optoelectronics, deep UV solar blind photodetectors, photodiodes, field emitters, or components for sensing and processing in harsh environments.[2,6–12] Amorphous gallium oxide, on the other hand, has been comparatively much less studied than the single- or poly-crystalline phases but has recently attracted attention, especially in the field of solar cells. Indeed, thin amorphous GaO_x layers have been shown to be an effective electron transport layer in CIGS- or CuO_2-based solar cells,[13,14] to act as an effective passivation layer for c-Si solar cells,[15] and to be an effective tunneling barrier to reduce electron recombination in dye-sensitized solar cells.[16] Amorphous gallium oxide could also be a potential gate oxide for metal-oxide-semiconductor devices particularly for GaN-based devices,[17] a tunneling barrier in dye sensitized solar cells,[16] a tunable channel in thin film phototransistors,[18] or act as a mixed ionic electronic conductor in memristive devices.[19]

For the deposition of gallium oxide thin films, various techniques are used, such as molecular beam epitaxy, sputtering, pulsed laser deposition, halide vapor phase epitaxy, metalorganic chemical vapor deposition, and atomic layer deposition (ALD).[2] The advantage

© Author(s) 2021

of ALD over other growth techniques lies in the precise thickness control and a conformal deposition on large areas due to the self-limiting nature of the deposition process. This is particularly true for the deposition of thin and ultrathin films. The thin film deposition of GaO_x by ALD has been pursued using different combinations of Ga precursors and oxygen sources, such as tri-dimethylamido gallium and water[16,20] or O_2 plasma,[21,22] dimethylgallium isopropoxide and water,[23] tetramethylheptanedionate gallium and O_2 plasma,[24] tri-isopropoxide and water,[25] trimethylgallium and ozone,[26,27] trimethylgallium and O_2 plasma,[15,28–33] triethylgallium and O_2 plasma,[17] and recently pentamethylcyclopentadienyl gallium and O_2 plasma.[34] In these studies, very little is reported on the electrical properties of the films, particularly on the leakage currents, as we will discuss later. Low level of leakage currents is a strong requirement for many nanoelectronic applications, and therefore it is key to understand how process parameters can help to reach this. The source of oxygen is most often oxygen plasma in ALD of gallium oxide. Although the oxygen plasma exposure time during each cycle might have a strong impact on the physical properties, there is, to the best of our knowledge, no report on the systematic variation of this parameter on the electrical properties.

In this paper, we focus on the effect of O_2 plasma exposure time on the dielectric permittivity and leakage current density J_L of amorphous gallium oxide films deposited by plasma-enhanced ALD. The electrical characterizations are complemented by *in situ* and *ex situ* spectroscopic ellipsometry analyses to understand how the SiO_x interfacial layer and the gallium oxide film evolve when increasing the O_2 plasma exposure up to 30 s.

II. EXPERIMENTS

Gallium oxide thin films were grown by plasma-enhanced atomic layer deposition (PEALD) on (100)-oriented p-type silicon wafers. The substrates were prepared using a standard RCA cleaning resulting in an ∼1.0 nm (±0.1 nm) chemical oxide SiO_x layer as determined by spectroscopic ellipsometry. The RCA clean consists of SC1 solution for 10 min at 80 °C (5:1:1 concentration ratio of deionized $H_2O + NH_4OH + H_2O_2$), followed by an HF dip for 15 s (HF 1%), and finally an SC2 solution for 10 min at 80 °C, (6:1:1concentration ratio of deionized $H_2O + HCl + H_2O_2$). We used either wafers of 200/100 mm diameter or pieces of $2.5 \times 2.5\ cm^2$ placed on a Si carrier wafer. The depositions were performed using an "Oxford FlexAl" ALD system with a remote plasma source and equipped with optical ports for *in situ* spectroscopic ellipsometry. Trimethylgallium $Ga(CH_3)_3$ (noted as TMGa) was used as a precursor, a remote coupled O_2 plasma as the oxidizing source, and Ar as a carrier or purge gas. The O_2 plasma was generated at 300 W with an O_2 flow of 60 SCCM. Each deposition cycle consisted of four steps: (1) TMGa precursor vapor pulse, (2) 100 SCCM Ar purging, (3) O_2 plasma gas generated with 60 SCCM O_2, and (4) 150 SCCM Ar purging. The pulse of O_2 plasma was triggered only when the pressure of 60 SCCM flowing O_2 was stabilized (15 mTorr). The thickness and optical index of the films were determined *ex situ* by spectroscopic ellipsometry (Woollam M2000) at three different incidence angles (60°, 65°, and 70°), in a wavelength range of 192–1690 nm. In order to avoid any assumption of optical dispersion law that would potentially lead to smoothing or loss of optical features, the optical fit was made in two steps. First, a wavelength-by-wavelength analysis[35] was made for modeling the gallium oxide layer (both the thickness and refractive index as fitting parameters) on a multisample analysis method,[36] while for the Si substrate and the 1.0 nm chemical oxide, we used referenced dispersions curves.[37] From this analysis, an optical model was then built to fit the same ellipsometric data. The same spectroscopic ellipsometer was used for *in situ* experiments during the growth with an incident angle of 70°. The data were recorded with 100 ms integration time. For these experiments, the grown film thickness was determined using the refractive index and absorption values of GaOx as determined *ex situ* for thicker amorphous films (>10 nm). The crystallinity was characterized by grazing incidence x-ray diffraction at 0.5° incidence (Cu K_α wavelength) using a Panalytical X-Pert MRD system.

The presence of carbon contamination in GaOx film was examined by x-ray photoelectron spectroscopy (XPS) using a monochromatized Al K_α x-ray source and a SPECS Phoibos 150 electron spectrometer. The high-resolution spectra were collected using a 15 eV pass energy with energy steps of 0.05 eV (takeoff angle of 35° with regard to the sample surface). To remove surface contamination, the sample surface was *in situ* sputtered in several subsequent steps by Ar^+ ions using a SPECS IQE 11/35 ion beam source. Electrical capacitance-voltage (C-V) and current-voltage (I-V) characterizations were performed on capacitive structures using a Keysight B1500A semiconductor parameter analyzer. Ni (10 nm)/Al (1 μm) top electrodes of 500 μm diameter were evaporated through a shadow mask.

III. RESULTS AND DISCUSSION

A. ALD process characterization

All films in this study are amorphous as shown by grazing incidence x-ray diffraction. Characteristics curves of the PE-ALD process are shown in Fig. 1. The deposition rate is found to be independent of the TMGa dosing time between 30 and 100 ms [Fig. 1(a)]; a value of 50 ms was chosen for all subsequent depositions. The O_2-plasma exposure time was varied between 0.5 and 30 s. A time of 3 s was identified as the lower limit for deposition in an ALD self-limited regime. As shown in Fig. 1(b), the growth per cycle (GPC) increases by ∼10% with plasma exposure time between 3 and 30 s, while at lower times the GPC is strongly reduced and clearly limited by the low flux of incoming oxygen species. Both purging times after TMGa dose and O_2-plasma were kept at 10 s to make sure the system was effectively purged, even though shorter (down to 2 s) or longer purge times did not affect the deposition rate. For a 3 s plasma exposure time, the GPC shows a constant value of 0.064 nm/cycle for the temperature range of 200–250 °C and of 0.068 nm/cycle at 100 °C [Fig. 1(d)]. For 8 s or longer plasma exposure times, the GPC at 200 °C is of ∼0.068–0.070 nm/cycle. These values are similar to those reported for processes using the same precursor and oxygen plasma source.[29,31,32] In Fig. 1(d), the linear evolution of the layer thickness for a deposition temperature of 200 °C shows the excellent stability of the process. As will be discussed later, hardly any change in the GPC is observed from the very beginning of the deposition process on a chemical oxide.

The uniformity achieved on 200 mm Si wafers is excellent. The spectroscopic ellipsometry mappings of the thickness and

© Author(s) 2021

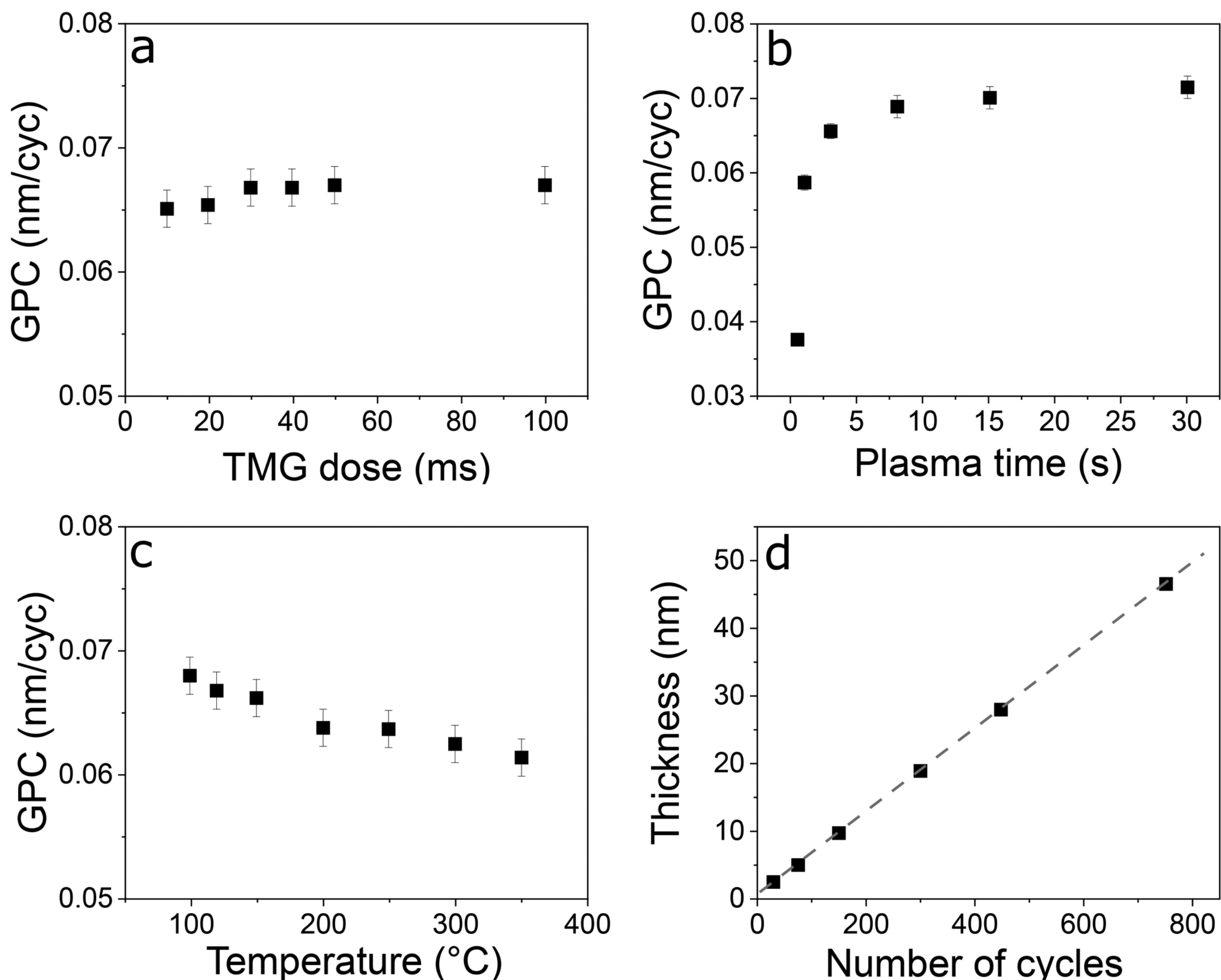

FIG. 1. GPC at 200 °C plotted as a function of (a) TMGa dosing time, (b) O_2 plasma exposure time, (c) temperature, and (d) film thickness (from spectroscopic ellipsometry) as a function of the number of cycles for deposition at 200 °C. For (a), (c), and (d), the O_2 plasma exposure time was 3 s.

refractive index for a wafer with ~46.5 nm GaO_x are shown in Figs. 2(a) and 2(b). The peak-to-peak thickness difference is 0.7 nm (1.5% of the average thickness of 46.45 nm), and the refractive index of 1.86 (at 632.8 nm) is deviating by less than 0.2%. The off-centering of the thickness along the diameter of the wafer in Fig. 2(a) corresponds to the fact that there is a single position of the precursor supply inlet in the chamber and not a radial inlet distribution (the highest thickness points toward the precursor inlet).

Spectroscopic ellipsometry measurements were performed *in situ* in order to probe the effect of the starting surface preparation on the growth. For ultrathin films, the nucleation stage is key in determining the final properties since a lack of uniform nucleation may lead to pin holes and island growth. In ALD, it is known that the growth, in the first cycles, depends strongly on the surface termination. For the deposition of metal oxides such as ZrO_2 or HfO_2, it was shown that −OH terminated surfaces are highly favorable while HF-last surfaces (−H terminated) lead to nucleation delay and island growth.[38–40] *In situ* ellipsometry is particularly suited for the study of the initial stages of the growth. Indeed, subtle changes occurring at the substrate's surface will induce, upon reflection of an incident polarized light, a change in its amplitude and phase. The data were recorded every 100 ms and fitted to determine the grown thickness with a model comprising a fixed SiO_2 interfacial layer (except for the HF-last surface) and a GaO_x film with a dispersion curve similar to that of an ~47 nm amorphous film measured *ex situ*. The GaO_x thickness was the only

© Author(s) 2021

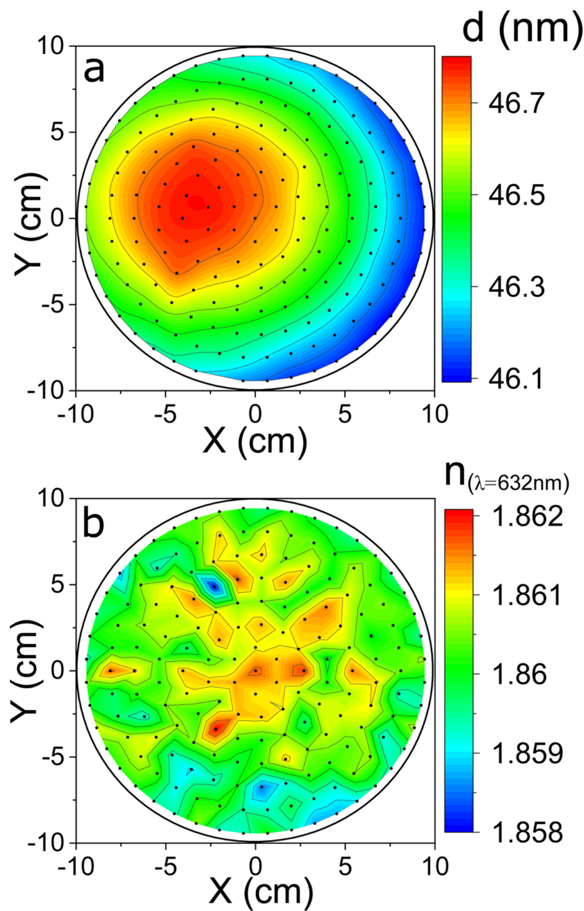

FIG. 2. Spectroscopic ellipsometry mapping of a 200 mm Si wafer coated with amorphous GaO_x. (a) Map of the thickness (46.45 ± 0.35 nm) and (b) refractive index at $\lambda = 632.8$ nm ($n = 1.860 \pm 0.002$).

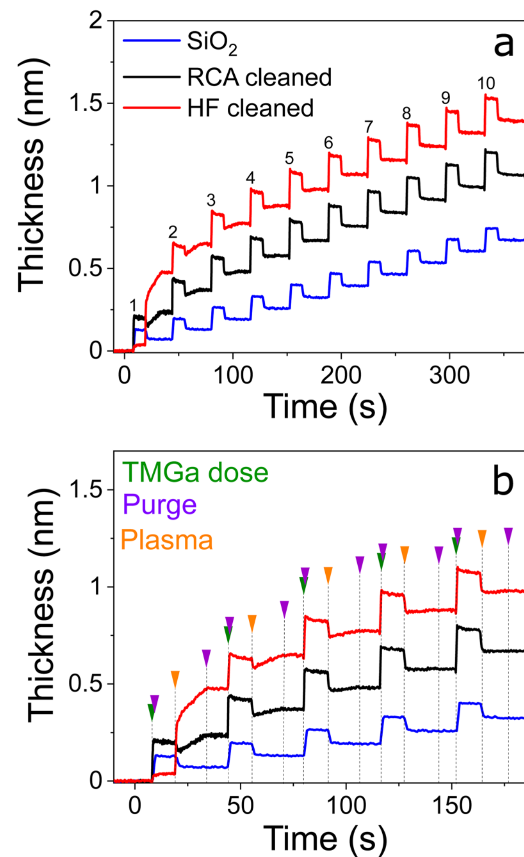

FIG. 3. (a) Thickness of the ALD-grown gallium oxide determined from *in situ* spectroscopic ellipsometry measurements as a function of time for depositions on three differently treated Si surfaces (HF-last, RCA cleaned with an ∼1 nm SiO_x chemical oxide, 300 nm thermally grown SiO_2). The plasma exposure time was 15 s at each cycle. (b) Zoom on the first five cycles of the growth.

fitting parameter. This model provides an effective grown thickness and does not take into account the different materials grown at every four steps of a cycle (TMGa exposure, purge, O_2 plasma exposure, and purge). The goal here, however, is to qualitatively study the effect of the starting surface.

In Fig. 3(a), the thickness of the grown GaO_x film is shown as a function of time over 10 cycles for three different starting surfaces: a chemical oxide of ∼1 nm after RCA clean, an HF-last surface, and a thermally grown 300 nm SiO_2. A steady-state growth (i.e., constant GPC) is observed from the very first cycle on thermally grown SiO_2, whereas it takes four cycles until a steady growth is established on the chemical oxide and five cycles on the HF-last surface. In the steady-state regime, the increase in thickness when the TMGa is introduced in the chamber occurs in ∼100 ms and corresponds to the adsorption of the precursor on available sites of the film surface. The thickness then remains constant during the purge step. When the surface is exposed to the oxygen plasma (for 15 s here), the thickness of the deposit decreases in less than 2 s and remains constant during the rest of the plasma exposure. During this step of the cycle, the methyl ligands are removed and the reaction of Ga atoms with oxygen occurs to form GaO_x. During the subsequent purge of oxygen, the thickness remains constant. The increase in thickness after each cycle is 0.11 nm on the RCA-cleaned surface. This value is larger than the expected one of ∼0.07 nm, which is due to the assumption that the optical index is the same as for thicker films, which is incorrect for ultrathin films below 1 nm. The lower growth per cycle (0.07 nm) determined on the thick thermal SiO_2 is fully consistent with similar observations reported for HfO_2 when comparing the growth on thermal SiO_2 and -OH rich chemical oxide surfaces.[39]

In Fig. 3(b), we highlight the five-first cycles and indicate the onset of each of the four steps in each cycle. On the HF-last surface, the first introduction of TMGa induces only a weak increase in apparent thickness, which shows an almost zero adsorption of TMGa on Si—H surface. The introduction of O_2 reactive species then provokes first a strong increase in the thickness

© Author(s) 2021

followed by a gradual increase in the thickness. In the following cycles, on both the HF-last and chemical oxide surfaces, the introduction of O_2 plasma leads, in less than 2 s, to a sharp decrease in the apparent thickness (as expected from the reaction of the TMGa precursor with oxygen) and then to its gradual increase during the first four and three cycles, respectively, until the purge step is started. This is not the case for the growth on the thick SiO_2 surface. This observation indicates that there is an interfacial SiO_x formation during the five and four first cycles of the deposition on the HF-last and chemical oxide surfaces, respectively. After these few initial cycles, oxygen does not reach the bottom interface with Si anymore and the oxidation of the interface stops. It also corresponds to the moment when the jump in apparent thickness after TMGa dosing becomes steady. Considering that after ~2 s of plasma exposure (on a total of 15 s at each cycle), only SiO_x grows, we calculated the SiO_x thickness grown at each cycle. The dispersions curves (n,k) used for the silicon oxides are the same as the one used for measuring the chemical oxide after surface preparation. After four cycles, the SiO_x thickness reaches a value of 1.27 nm (for a starting chemical oxide of 1.00 ± 0.05 nm). In Sec. III B, we study the effect of the plasma exposure time on the SiO_x regrowth starting from standard RCA-cleaned chemical oxide Si substrates.

B. Influence of the O_2 plasma exposure time on the interfacial regrowth

In situ ellipsometry was performed for increasing oxygen plasma exposure times up to 30 s and the resulting calculated thicknesses of the GaO_x film (determined as previously explained) are shown in Fig. 4(a) for the first four cycles. The strong increase in apparent thickness after TMGa dosing is followed by a strong decrease when the O_2 plasma is introduced due to the reaction with the TMGa adsorbed molecules with a net increase in the total GaO_x thickness corresponding to the growth per cycle. During the 1 or 3 s O_2 plasma steps, no thickness increase is observed, which indicates that there is no detectable growing interfacial SiO_x at these low exposure times. On the contrary, during the 8, 15, and 30 s O_2 plasma exposure steps, for the first three cycles, the thickness continuously increases which is due to the SiO_x interfacial regrowth. From the fourth cycle, it then stays constant, indicating that no additional oxygen reaches the bottom interface. The thickness evolution of the growing SiO_x while exposing the surface to the O_2 plasma is calculated from the ellipsometry data [Fig. 4(b)] and the resulting total interface thickness is shown for the different exposure times in Fig. 4(c). The overall regrowth of the interfacial SiO_x under prolonged oxygen plasma exposure is limited to 0.27 nm.

C. Influence of the O_2 plasma exposure time on electrical and optical properties of GaOx

A typical capacitance-voltage (C-V) curve measured on an Al/Ni/30 nm GaO_x/SiO_x/p-Si capacitor is shown in Fig. 5(a) for a GaO_x film deposited using 30 s O_2 plasma exposure time. The shift observed between the different frequencies for positive voltage is attributed to the presence of interfacial traps in the GaO_x layer. The relative (static) dielectric permittivity ϵ_r of GaO_x was calculated from the capacitance in accumulation and taking into account the SiO_x interfacial layer contribution ($\epsilon_{rSiO2} =$ 3.9 and thickness

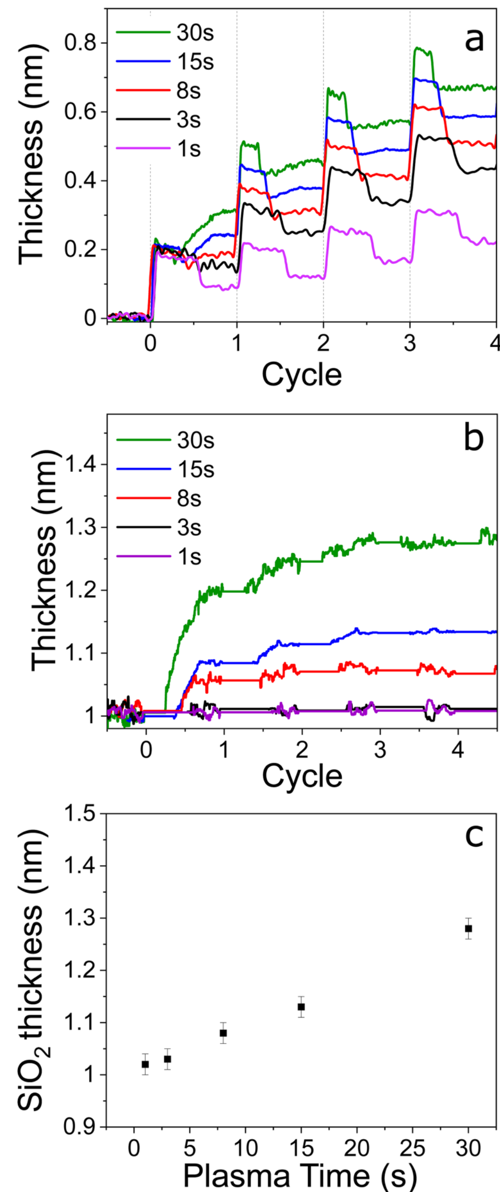

FIG. 4. (a) Thickness of the ALD-grown gallium oxide GaO_x determined from *in situ* spectroscopic ellipsometry measurements as a function of the number of cycles for depositions performed with different O_2 plasma exposure times. (b) Thickness of the interfacial SiO_x formed when O_2 plasma is introduced at each cycle, determined from *in situ* spectroscopic ellipsometry measurement as a function of the number of cycles during depositions using different O_2 plasma exposure times. (c) Thickness of the interfacial SiO_x as a function of the O_2 plasma exposure time determined from *in situ* spectroscopic ellipsometry.

as determined by ellipsometry). We observe a strong dependence of the dielectric permittivity of GaO_x with the plasma exposure time as shown in Fig. 5(b). From 3 to 8 s O_2 plasma, the relative permittivity ϵ_r is 9.6–9.8 ± 0.4 and then it increases continuously up to

© Author(s) 2021

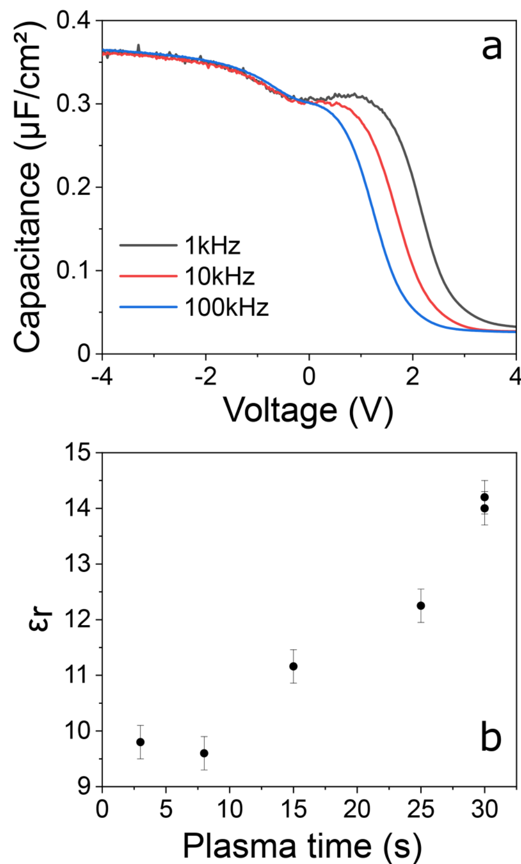

FIG. 5. (a) Capacitance as a function of applied voltage measured at three different frequencies on an Al/Ni/GaO_x/SiO_x/Si capacitor with 30.0 nm GaO_x film (30 s O_2 plasma exposure time during deposition). (b) Relative dielectric permittivity of GaO_x as a function of oxygen plasma exposure time.

14.2 ± 0.2 for 30 s plasma exposure times. This value is larger than most values reported for amorphous films. For ALD films, Choi *et al.* measured $\epsilon_r = 9.2$ for 40 nm film[25] and Li *et al.* measured $\epsilon_r = 11.9$.[32] Passlack *et al.* measured ϵ_r of 9.93 ± 0.39 ($T_s = 40$ °C with no additional oxygen) and 10.2 ± 0.6 ($T_s = 125$ °C, O_2 partial pressure of 2×10^{-4} Torr) for amorphous films grown by sputtering.[41] A noticeable high ϵ_r of 16 has been measured by Qin *et al.* for 200 nm amorphous Ga_2O_3 films grown by sputtering (see the supplementary material of Ref. 18). The ϵ_r value of 14.2 ± 0.2 that we measure for large O_2 plasma exposure times is larger than any of the values of single crystalline β-Ga_2O_3 [10.2 ± 0.2, 10.87 ± 0.08, and 12.4 ± 0.4 for directions perpendicular to the planes (100), (010), and (001), respectively].[42] The static dielectric permittivity can be decomposed into an electronic contribution ε_∞ and a lattice contribution ε_{ion} (contributions of the IR-active phonon modes). In some cases, an amorphous phase may have a larger static dielectric permittivity than that of its single crystalline counterpart stable at room temperature and atmospheric pressure due to a larger ionic component contribution to the permittivity. This is the case for the sesquioxide Sc_2O_3, which has been predicted by density functional theory (DFT) calculations to exhibit an enhanced permittivity in the amorphous state ($\epsilon_r \sim 22$) compared to the one in the cubic bixbyite crystal structure ($\epsilon_r \sim 15$).[43] This boosted permittivity is attributed by Delugas *et al.* to the conservation of polarizability in the amorphous phase together with a disorder-induced IR activation of nonpolar low-energy modes related to cation-oxygen combined motions.[43] Amorphous HfO_2 ($\epsilon_r \sim 20-25$) is another example of an enhanced permittivity compared to the monoclinic phase ($\epsilon_r \sim 16$), which is the stable phase at room temperature and atmospheric pressure, while higher symmetry phases (such as cubic, tetragonal, or orthorhombic) have larger permittivities.[44–46] The enhanced permittivity in our GaO_x films compared to the one of

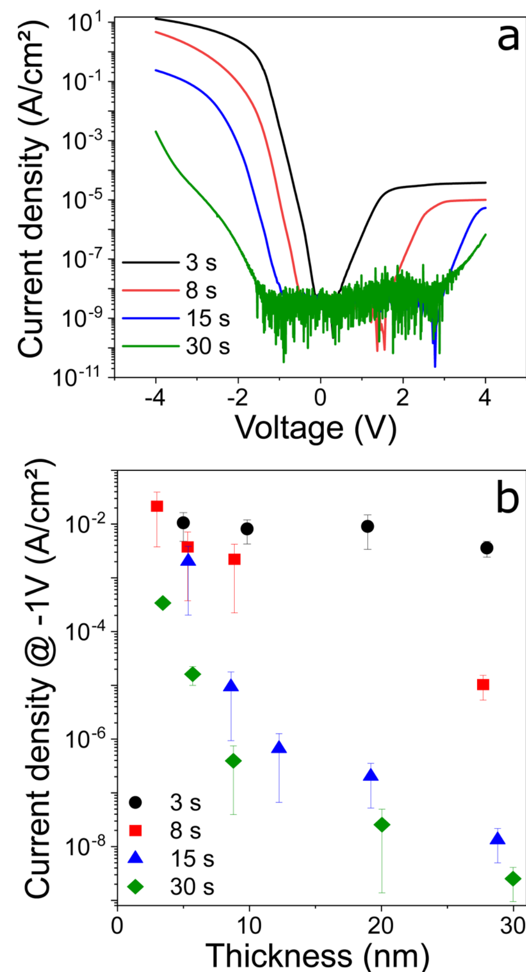

FIG. 6. Leakage currents in Al/Ni/GaO_x/SiO_x/Si capacitors prepared with different O_2 plasma exposure times. (a) Leakage current density as a function of applied voltage for ∼30 nm GaO_x films grown on p-type Si (001) by ALD using different O_2 plasma times. (b) Evolution of the leakage current density measured at −1 V as a function of the GaO_x film thickness for various plasma times.

© Author(s) 2021

β-Ga_2O_3 could originate from a change in the local order when the O_2 plasma exposure is increased to long times. Recently, Yusa *et al.* have determined the permittivity of epitaxial films ϵ-Ga_2O_3 (deposited on a conducting indium tin oxide bottom electrode on yttria-stabilized zirconia substrate) and found values of $\epsilon_r = 14$ for a 89 nm film and $\epsilon_r = 32.1$ for a 136 nm film.[47] Further investigations by scanning transmission electron microscopy might help to give insights into the local structure of the films grown under different O_2 plasma exposure times.

The leakage current density as a function of applied voltage is shown in Fig. 6(a) for 30 nm films prepared with different O_2 plasma exposure times. For positive voltages, the diodelike behavior observed for 3 and 8 s exposure is attributed to the p-n junction formed between GaO_x and silicon. The effect of the plasma time on the leakage currents is particularly strong for low bias voltages (typically −1 V). A decrease of more than 5 orders of magnitude of the leakage current density between 3 s plasma time and 30 s plasma time is observed for 30 nm films, from 3.6×10^{-3} A/cm^2

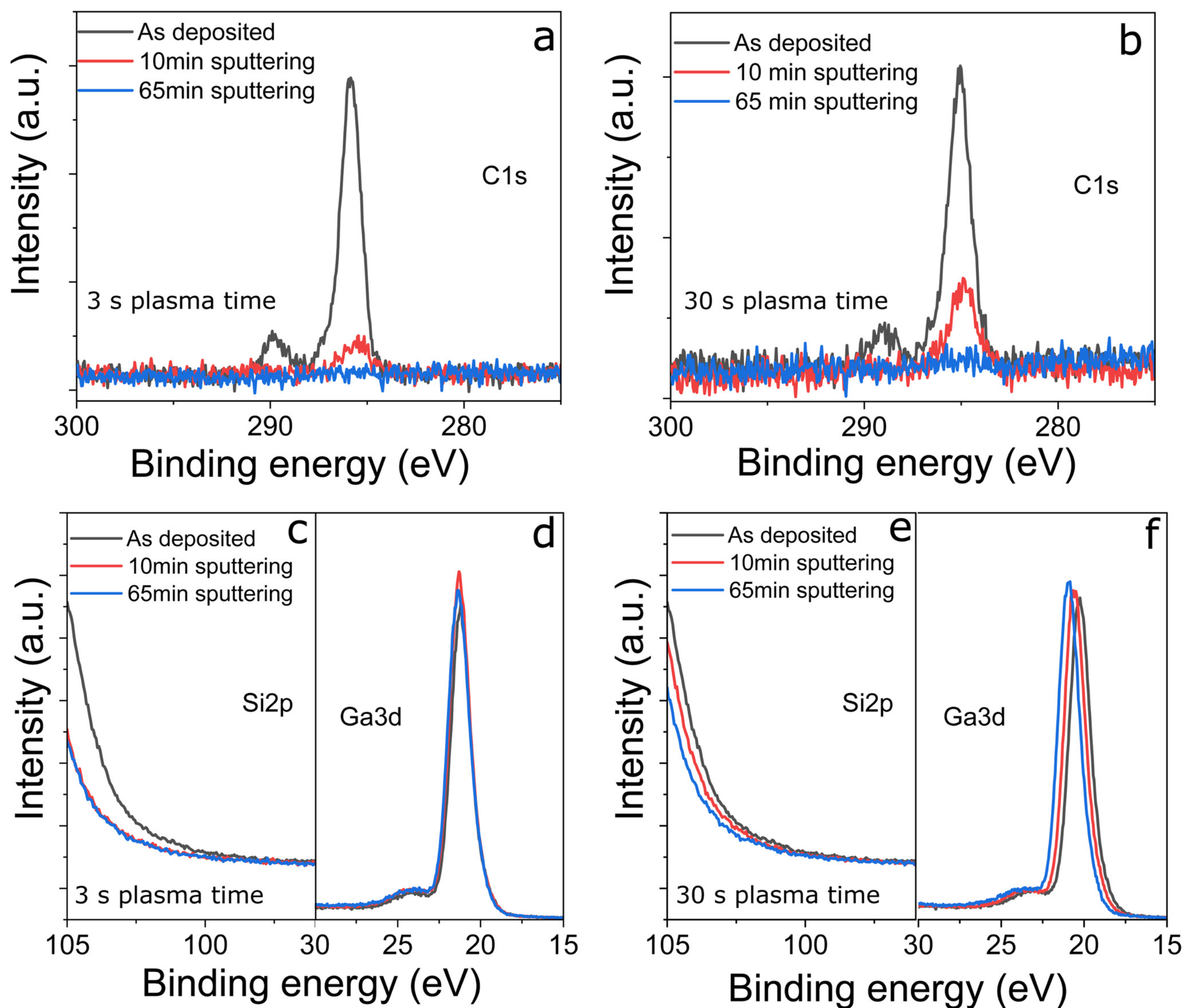

FIG. 7. XPS spectra recorded on amorphous GaO_x films, as-deposited, and after a total of 10 and 65 min of *in situ* Ar^+ sputtering (5 + 5 min at 1 keV, 1×10^{-5} mbar, followed by 5 + 10 + 30 min at 5 keV, 1.3×10^{-5} mbar). For the 3 s O_2-plasma-time film, the XPS spectra are (a) C 1s, (c) Si 2p, and (d) Ga 3d. For the 30-s O_2-plasma-time film, the XPS spectra are (b) C 1s, (e) Si 2p, and (f) Ga 3d.

© Author(s) 2021

down to 2.5×10^{-8} A/cm^2 respectively. The decrease in leakage currents with increasing plasma time is observed for all thicknesses, as shown in Fig. 6(b). For 8 nm, the gain is still of 4 orders of magnitude between 3 and 30 s plasma times. The trend observed as a function of thickness for the leakage current both at a given plasma time and for increasing plasma times is consistent with bulk defects being involved in the conduction mechanisms and these bulk defects concentration being strongly decreased with longer O_2 plasma exposure times.

A recent study reports the presence of carbon in PEALD-grown amorphous GaO_x films in a quite large amount (15.9% for films grown at 200 °C).[33] For our films, it could be suspected that the O_2 plasma time has a strong impact on the incorporated carbon during deposition. C could be incorporated from the TMGa precursor which has three C atoms for one Ga atom. In order to clarify this point, XPS measurements were performed on two 30 nm-thick GaO_x samples prepared with 3 or 30 s O_2 plasma times. First, the C 1s core level spectrum was measured on each as-deposited film. Then, each sample was sputtered *in situ* multiple times (Ar^+ ions) to record the corresponding evolution of the carbon peak. To make sure that we had reached the bulk of the film but that we did not etch it out completely, we sputtered until Si 2p could be observed while still being able to detect the Ga 3d contribution. The sputtering rate was relatively low and it took more than 155 min to detect the Si 2p peak. Three XPS spectra are presented in Fig. 7 (as-deposited, and after 10 and 65 min sputtering).

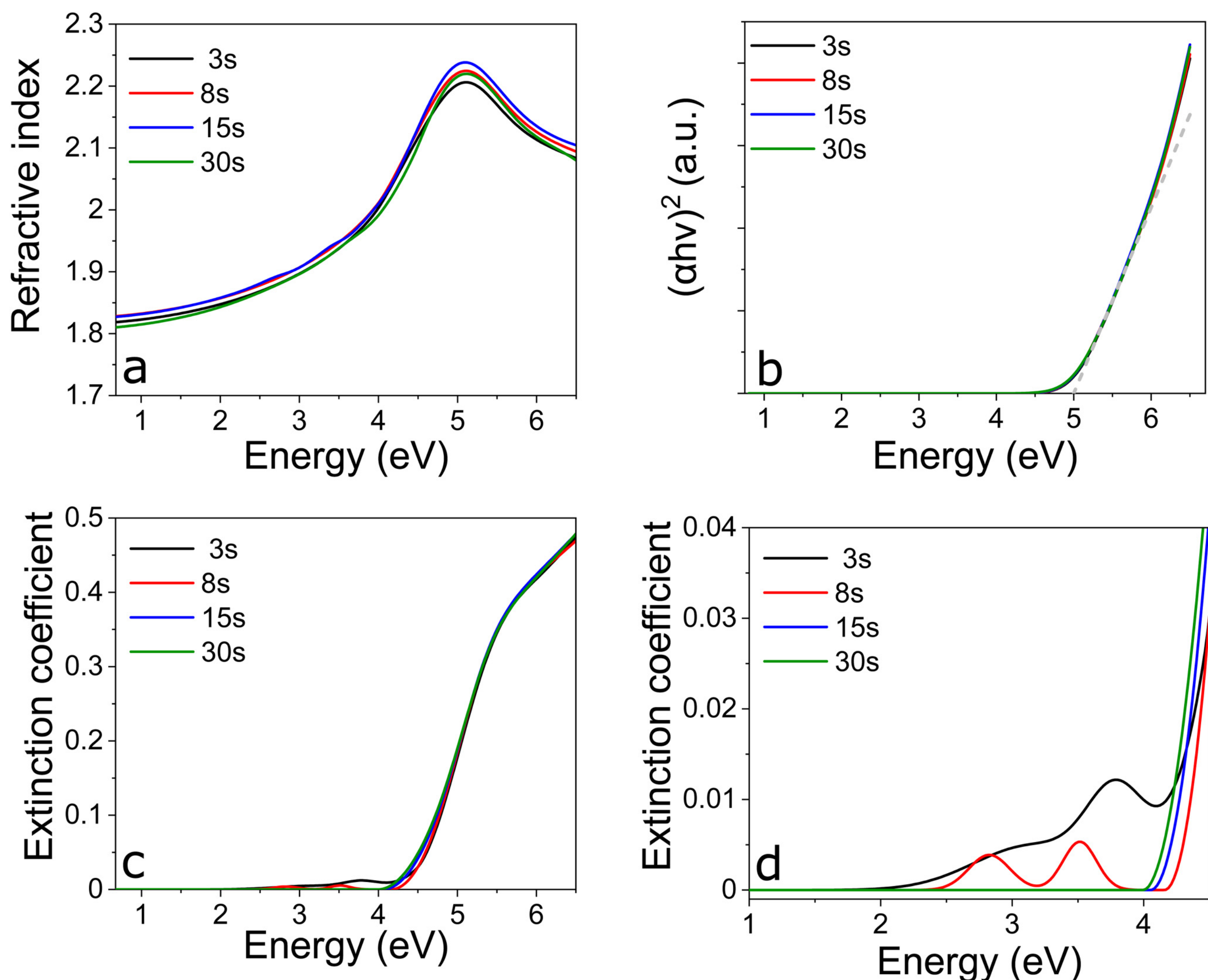

FIG. 8. Optical properties derived from *ex-situ* spectroscopic ellipsometry on GaOx films (10–20 nm) deposited by PEALD using different O_2 plasma exposure times: (a) refractive index, (b) Tauc plot, (c) extinction coefficient, and (d) a zoom of the extinction coefficient in the 1.0–4.5 eV range.

© Author(s) 2021

For the as-deposited films, the C 1s peak observed at ~285–286 eV is attributed to hydrocarbon species with C—H or C—C bonds, while the peak of lower intensity at ~290 eV is attributed to oxidized carbonaceous species with C—O—C or O—C═O bonds [Figs. 7(a) and 7(b)].[48] Both contributions disappear completely after sputtering the samples for 15 min and in all subsequent sputtering steps, which indicates that they originate from surface contamination—the so-called adventitious carbon—that is typical for air-exposed surfaces (see Figs. 7(a) and 7(b) for 65 min sputtering).[48] Furthermore, the Ga 3d peak and the absence of Si 2p peak [Figs. 7(c)–7(f)] confirm that the gallium oxide film is still present and thick enough that the substrate's contribution cannot be measured. The tail that is observed in the Si 2p spectra arises from the Ga 3p peak at ~106.5 eV (not shown). After 155 min, a Si 2p contribution from the substrate (Si—Si) and from the SiO_x (Si—O) interface was detected. These measurements confirm that no carbon contamination can be observed in our films whatever the O_2 plasma exposure time is (in the range of 3–30 s) within the detection level of ~0.1%. One cannot preclude that lower amounts of C are present in the films (below 1000 ppm).

For further investigation of the defects in the films, *ex-situ* spectroscopic ellipsometry was performed. In previous reports on GaO_x films, the spectroscopic ellipsometry data are treated using the conventional Tauc–Lorentz or Cody models. However, these models do not allow to reproduce the behavior for energies below the bandgap. To improve the data modeling particularly below the bandgap energy where the signal recorded is close to the detection limit, a multisample analysis method combined with wavelength-by-wavelength fits has been performed to determine n and k values (wavelength by wavelength) to guide then the optical model used. A model made of two Tauc–Lorentz oscillators, accounting for the bandgap dispersion of the material, and two Gaussians, accounting for absorption below the bandgap, was used to fit the ellipsometric data. The information gained is shown in Fig. 8. Small differences arise in the refractive index [Fig. 8(a)] with no clear trend with the plasma time, suggesting only a minor influence of the plasma time on the refractive index and hence on the electronic component ε_∞ of the static dielectric permittivity. The optical bandgap, extracted from a linear expansion of the Tauc plot [Fig. 8(b)], is found to be constant for all plasma times, with $E_g = 4.97 \pm 0.1$ eV. This value is slightly larger than values reported in the literature using ellipsometry as well (4.68 eV for PEALD).[5] The extinction coefficient appears independent of the plasma time for energies values above the bandgap [Fig. 8(c)]. However, the data analysis below the bandgap in the 2–4.5 eV range [Fig. 8(d)] evidences the presence of two broad absorption bands for the lower plasma times of 3 and 8 s. These absorptions bands can be attributed to oxygen vacancy states which are typical point defects in Ga_2O_3 that are located at energies of ~2.75 and 3.6 eV as predicted by DFT calculations and are likely to form in under-oxidized GaO_x.[49–51] It can be observed that the peak intensities characteristics of these defects decrease for increasing plasma times from 3 to 8 s and then reach a value lower than the measurement limit for plasma exposure times of 15 and 30 s. Hence, from this optical study, we show that a longer plasma exposure time clearly allows to reduce oxygen vacancies in the GaO_x films even though a lower plasma time suffices to reach the ALD window regime for the growth. The presence of a significant amount of oxygen vacancies as evidenced by optical measurements is thought to explain the large leakage currents measured for plasma exposure times below 15 s.

IV. SUMMARY AND CONCLUSIONS

Amorphous GaO_x thin films were deposited on Si (001) substrates by plasma-enhanced ALD. The effect on the electrical properties of the oxygen plasma exposure time during each cycle was investigated. The amorphous films grown at oxygen plasma times of a few seconds (typically 3–8 s) exhibit large leakage current densities ($J_L = 3.6\ 10^{-3}$ A/cm^2 at −1 V for 30 nm film) that can be dramatically reduced ($J_L = 2.5 \times 10^{-8}$ A/cm^2 at −1 V for 30 nm film) by increasing the exposure time up to 15–30 s, well above the value that is required to reach a stable growth per cycle. Optical measurements evidence two absorption bands below the bandgap that are associated with the presence of oxygen vacancies. These absorptions are no more observed for long O_2 plasma exposure times (15–30 s). The reduction of the leakage current density is clearly associated with a significant decrease in oxygen vacancies concentration in the amorphous films. Moreover, a continuous increase in the static dielectric permittivity is observed with increasing O_2 plasma time, reaching a value of $\varepsilon_r = 14.2$ for 30 s exposure. This enhanced permittivity might originate from a change in the local ion order approaching that of the ε-Ga_2O_3 phase. With this study, we show that the O_2 plasma exposure time during the ALD process provides a path toward controlling the intrinsic doping of amorphous ALD-grown GaO_x films to obtain, on the one hand, fully insulating films with tunable dielectric permittivity or, on the other hand, semiconducting films with tunable oxygen deficiency and therefore tunable carrier concentration.

ACKNOWLEDGMENT

This work was performed in the framework of GraFOx II, a Leibniz-Science Campus. H.K. and F.M. contributed equally to this work.

DATA AVAILABILITY

The data that support the findings of this study are available from the corresponding authors upon reasonable request.

REFERENCES

[1] R. Roy, V. G. Hill, and E. F. Osborn, J. Am. Chem. Soc. **74**, 719 (1952).
[2] S. J. Pearton, J. Yang, P. H. Cary IV, F. Ren, J. Kim, M. J. Tadjer, and M. A. Mastro, Appl. Phys. Rev. **5**, 011301 (2018).
[3] Z. Galazka *et al.*, Cryst. Res. Technol. **45**, 1229 (2010).
[4] Z. Galazka *et al.*, J. Cryst. Growth **404**, 184 (2014).
[5] A. Kuramata, K. Koshi, S. Watanabe, Y. Yamaoka1, T. Masui, and S. Yamakoshi, Jpn. J. Appl. Phys. **55**, 1202A2 (2016).
[6] M. Higashiwaki and G. H. Jessen, Appl. Phys. Lett. **112**, 060401 (2018).
[7] M. Higashiwaki, K. Sasaki, A. Kuramata, T. Masui, and S. Yamakoshi, Phys. Status Solidi A **211**, 21 (2014).
[8] H. Xue, Q. He, G. Jian, S. Long, T. Pang, and M. Liu, Nanoscale Res. Lett. **13**, 290 (2018).
[9] E. Chikoidze *et al.*, Mater. Today Phys. **3**, 118 (2017).
[10] X. Wang, Z. Chen, D. Guo, X. Zhang, Z. Wu, P. Li, and W. Tang, Opt. Mater. Express **8**, 2918 (2018).

© Author(s) 2021

[11]A. Grillo *et al.*, Appl. Phys. Lett. **114**, 193101 (2019).
[12]X. Chen, F. Ren, S. Gu, and J. Ye, Photonics Res. **7**, 381 (2019).
[13]T. Minami, Y. Nishi, and T. Miyata, Appl. Phys. Express **6**, 044101 (2013).
[14]T. Koida, Y. Kamikawa-Shimizu, A. Yamada, H. Shibata, and S. Niki, IEEE J. Photovoltaics **5**, 956 (2015).
[15]T. G. Allen, M. Ernst, C. Samundsett, and A. Cuevas, *2015 IEEE 42nd Photovoltaic Specialist Conference (PVSC)*, New Orleans, LA, New Orleans, LA, 14-19 June (IEEE 2015), pp. 1–6.
[16]A. K. Chandiran, N. Tetreault, R. Humphry-Baker, F. Kessler, E. Baranoff, C. Yi, M. K. Nazeeruddin, and M. Gratzel, Nano Lett. **12**, 3941 (2012).
[17]H.-Y. Shih, F.-C. Chu, A. Das, C.-Y. Lee, M.-J. Chen, and R.-M. Lin, Nanoscale Res. Lett. **11**, 235 (2016).
[18]Y. Qin *et al.*, Adv. Electron. Mater. **5**, 1900389 (2019).
[19]A. Yoshitaka, C. Wiemann, V. Feyer, H.-S. Kim, C. M. Schneider, H. Ill-Yoo, and M. Martin, Nat. Commun. **5**, 3473 (2014).
[20]C. L. Dezelah, IV, J. Niinistö, K. Arstila, L. Niinistö, and C. H. Winter, Chem. Mater. **18**, 471 (2006).
[21]G. X. Liu, F. K. Shan, J. J. Park, W. J. Lee, G. H. Lee, I. S. Kim, B. C. Shin, and S. G. Yoon, J. Electroceram. **17**, 145 (2006).
[22]R. O'Donoghue, J. Rechmann, M. Aghaee, D. Rogalla, H.-W. Becker, M. Creatore, A. D. Wieck, and A. Devi, Dalton Trans. **46**, 16551 (2017).
[23]H. Lee, K. Kim, J.-J. Woo, D.-J. Jun, Y. Park, Y. Kim, H. W. Lee, Y. J. Cho, and H. M. Cho, ECS Trans. **25**, 587 (2009).
[24]R. K. Ramachandran, J. Dendooven, J. Botterman, S. P. Sree, D. Poelman, J. A. Martens, H. Poelman, and C. Detavernier, J. Mater. Chem. A **2**, 19232 (2014).
[25]D. Choi, K.-B. Chung, and J.-S. Park, Thin Solid Films **546**, 31 (2013).
[26]D. J. Comstock and J. W. Elam, Chem. Mater. **24**, 4011 (2012).
[27]T. G. Allen and A. Cuevas, Appl. Phys. Lett. **105**, 031601 (2014).
[28]I. Donmez, C. Ozgit-Akgun, and N. Biyikli, J. Vac. Sci. Technol. A **31**, 01A110 (2013).
[29]H. Altuntas, I. Donmez, C. Ozgit-Akgun, and N. Biyikli, J. Alloys Compd. **593**, 190 (2014).
[30]T. G. Allen and A. Cuevas, Phys. Status Solidi RRL **9**, 220 (2015).
[31]P. P. Pansila, K. Kanomata, B. Ahmad, S. Kubota, and F. Hirose, IEEE Trans. Electron. **E98.C**, 382 (2015).
[32]X. Li, H.-L. Lu, H.-P. Ma, J.-G. Yang, J.-X. Chen, W. Huang, Q. Guo, J.-J. Feng, and D. W. Zhang, Curr. Appl. Phys. **19**, 72 (2019).
[33]A. Mahmoodinezhad, C. Janowitz, F. Naumann, P. Plate, H. Gargouri, K. Henkel, D. Schmeisser, and J. I. Flege, J. Vac. Sci. Technol. A **38**, 022404 (2020).
[34]F. Mizutani, S. Higashi, M. Inoue, and T. Nabatame, J. Vac. Sci. Technol. A **38**, 022412 (2020).
[35]D. E. Aspnes, J. Vac. Sci. Technol. A **31**, 058502 (2013).
[36]J. N. Hilfiker, N. Singh, T. Tiwald, D. Convey, S. M. Smith, J. H. Baker, and H. G. Tompkins, Thin Solid Films **516**, 7979 (2008).
[37]C. M. Herzinger, B. Johs, W. A. McGahan, J. A. Woollam, and W. Paulson, J. Appl. Phys. **83**, 3323 (1998).
[38]M. Copel, M. Gribelyuk, and E. Gusev, Appl. Phys. Lett. **76**, 436 (2000).
[39]M. L. Green *et al.*, J. Appl. Phys. **92**, 7168 (2002).
[40]L. Nyns *et al.*, J. Electrochem. Soc. **153**, F205 (2006).
[41]M. Passlack, N. E. J. Hunt, E. F. Schubert, G. J. Zydzik, M. Hong, J. P. Mannaerts, R. L. Opila, and R. J. Fischer, Appl. Phys. Lett. **64**, 2715 (1994).
[42]A. Fiedler, R. Schewski, Z. Galazka, and K. Irmscher, ECS J. Solid State Sci. Technol. **8**, Q3083 (2019).
[43]P. Delugas, V. Fiorentini, and A. Filippetti, Appl. Phys. Lett. **92**, 172903 (2008).
[44]G.-M. Rignanese, J. Phys.: Condens. Matter **17**, R357 (2005).
[45]F. Ducroquet, E. Rauwel, V. Brizé, and C. Dubourdieu, ECS Trans. **28**, 191 (2010).
[46]Y. Wang, F. Zahid, J. Wang, and H. Guo, Phys. Rev. B **85**, 224110 (2012).
[47]S. Yusa, D. Oka, and T. Fukumura, CrystEngComm **22**, 381 (2020).
[48]T. L. Barr and S. Seal, J. Vac. Sci. Technol. A **13**, 1239 (1995).
[49]L. Dong, R. Jia, B. Xin, B. Peng, and Y. Zhang, Sci. Rep. **7**, 40160 (2017).
[50]X. Ma, Y. Zhang, L. Dong, and R. Jia, Results Phys. **7**, 1582 (2017).
[51]M. D. McCluskey, J. Appl. Phys. **127**, 101101 (2020).

© Author(s) 2021